論　文

NETSUSOKUTEI 5(1) 11–18 (1978)

The Thermal Conductivity and Diffusivity of $Mn_xFe_{3-x}O_4$ ($0 \leqq x \leqq 1.5$) from 200 to 700 K

Yasuo Noda and Keiji Naito

(Received 9 September, 1977)

Abstract

The thermal conductivity of $Mn_xFe_{3-x}O_4$ with various compositions (x = 0, 0.25, 0.5, 0.8, 1.0, 1.5) and hematite, and the thermal diffusivity of $Mn_xFe_{3-x}O_4$ (x = 0.8, 1.0, 1.5) were measured by means of a scanning temperature method in the temperature range from 200 to 700 K. An anomaly of ferrimagnetic transition was observed in the thermal diffusivity measurement for each sample, and the peak temperatures varied with the composition (x = 0.8, 1.0, 1.5) were in good agreement with those observed in the permeability measurements. The anomaly was not as clearly observed in the thermal conductivity measurement as in the thermal diffusivity measurement. The measured values for thermal conductivity of $Mn_xFe_{3-x}O_4$ were so low that the phonon mean free paths calculated from the thermal conductivity data were comparable with the lattice constant. The thermal conductivity of $Mn_xFe_{3-x}O_4$ was strongly dependent on composition x and showed the maxima at the compositions with x = 0 and 1.0.

1. Introduction

The metal ions in a compound with spinel-type structure are distributed in the tetrahedral and octahedral sites, and the cation distribution influences on its physical properties. The cation distribution in manganese ferrites $Mn_xFe_{3-x}O_4$ has been determined by means of magnetic susceptibility[1–4], X-ray diffraction[5,6] and infra-red absorption studies[6,7]. In the region $0 \leqq x \leqq 1.9$, the compounds of the type $Mn_xFe_{3-x}O_4$ are cubic. At x = 0, the structure is that of the inverse spinel type $Fe^{3+}(Fe^{2+}Fe^{3+})O_4$, where cations in brackets occupy octahedral sites and the others tetrahedral sites. As x increases from 0 to 1.0, the Mn^{2+} ions replace the Fe^{3+} ions on the tetrahedral sites. At x = 1 the structure becomes that of the intermediate spinel type $Mn^{2+}_{0.8}Fe^{3+}_{0.2}(Mn^{2+}_{0.2}Fe^{3+}_{1.8})O_4$. As x becomes larger than 1.0, Mn^{3+} ions replace the Fe^{3+} ions and the Mn^{2+} ions on the octahedral sites. In the region $x > 1.9$, the structure becomes tetragonal by the Jahn-Teller distortion of Mn^{3+} ions in octahedral sites[6].

The thermal conductivity of $MnFe_2O_4$ single crystal was reported by Shchelkotunov *et al.* in the temperature range from 200 to 670 K[8]. They observed linear relationship between thermal resistance and $1/T$, and the slope changes slightly at the magnetic transition temperature, above which the slope becomes smaller. And they have concluded that the phonon contribution is dominant in the thermal conductivity of $MnFe_2O_4$. Douthett *et al.* reported the thermal conductivity of $MnFe_2O_4$ single crystal over the temperature range from 1.4 to 25 K[9], and pointed out that the magnon contribution to thermal conductivity is negligibly small compared with phonon contribution, although the phonon is scattered by magnon.

In this study, the thermal conductivity and diffusivity of $Mn_xFe_{3-x}O_4$ with x from 0 to 1.5 and Fe_2O_3 were measured continuously by a scanning temperature method[10,11] in the temperature range from 200 to 700 K, and the effect of the metal composition upon these thermal properties and also the change due to the magnetic transition are to be discussed.

Department of Nuclear Engineering, Faculty of Engineering, Nagoya University, Furo-cho, Chikusa-ku, Nagoya, Japan

2. Experimental

2.1 Sample

The pellets for hematite and magnetite were prepared by pressing pure α-Fe_2O_3 in a 10 mm circular die at about 2000 kg/cm^2. For $Mn_xFe_{3-x}O_4$ ($0.5 \leqq x \leqq 1.5$), the mixture of α-Fe_2O_3 and $MnCO_3$ powder in an appropriate metal composition was prefired for 3 h at 600℃ and then pressed in the same die at the same pressure. The pellets for hematite and magnetite were sintered for 50 h at 1300℃ in air and in argon, respectively. The pellets for $Mn_xFe_{3-x}O_4$ ($0.5 \leqq x \leqq 1.5$) were sintered for 50 h at 1300℃ in air. In order to obtain the exact metal-oxygen ratio of 3:4, the magnetite samples were refired at oxygen partial pressure of about 10^{-9} atm in the mixture of H_2/CO_2 = 1/100 for 15 h at 1050℃, refering to the oxygen potential-temperature diagram of magnetite[12], and the $Mn_xFe_{3-x}O_4$ samples (x = 0.8, 1.0, 1.5) at oxygen partial pressure of about 10^{-5} atm for 15 h at 1050℃ and the $Mn_{0.5}Fe_{2.5}O_4$ samples at 1100℃, refering to oxygen potential-temperature diagram of manganese ferrites[13-15]. The pellet of $Mn_{0.25}Fe_{2.75}O_4$ was difficult to obtain in a dense form by this method, then FeO powder was added to the prefired mixture of α-Fe_2O_3 and $MnCO_3$ powder in an appropriate ratio before pressing, and the pellet heated in oxygen partial pressure of about 10^{-9} atm in the mixture H_2/CO_2 = 1/100 for 15 h at 1050℃.

The sintered pellets obtained (8~9 mm diameter and 2~5 mm thickness) were finely polished into a cylindrical shape with silicon carbide papers. After the measurement of thermal conductivity and diffusivity, the sample composition was determined by measurement of the lattice parameter[6,16] and the composition determined was in good agreement with the initial Mn/Fe ratio. Initial Mn-Fe composition (x), X-ray diffraction pattern and lattice constant, density and porosity are shown in Table 1.

2.2 Measurement of thermal conductivity and diffusivity

The apparatus and measurement of the thermal conductivity and diffusivity by scanning temperature method has been described in detail previously[10,11]. In this method, thermal properties, such as thermal conductivity and diffusivity, can be obtained continuously from measurement of the temperature difference ΔT between the lower surface (heating surface) and the upper one of cylindrical samples at quasi-steady state during heating at a constant rate, β. Thermal conductivity λ and diffusivity κ can be shown by the following equation (1) and (2), respectively[11],

$$\lambda = (YC_s\rho_s + Z)/(\Delta T/\beta - X) \quad (1)$$

$$\kappa = (Y + Z/C_s\rho_s)/(\Delta T/\beta - X) \quad (2)$$

where $Y = l^2/2$, $Z = (C_M M_M - K_L \Delta T/\beta)l/S$, $X = 2R(C_M M_M - K_L \Delta T/\beta) + C_s M_s R$; l, S, C_s, M_s, and ρ_s are length, cross section, specific heat capacity, weight and density of sample; C_M and M_M specific heat capacity and weight of silver block acting as thermal sink, respectively; K_L the heat leakage

Table 1. $Mn_xFe_{3-x}O_4$ Samples

Sample No.	initial Mn-Fe composition x	X ray		density g cm^{-3}	porosity, %
		lattice constant/Å	pattern		
1	0	8.398 ±0.0007	magnetite	4.25	18
2	0.25	8.436 ±0.0008	cubic spinel single phase	4.48	12
3	0.5	8.466 ±0.0015	cubic spinel single phase	4.05	20
4	0.8	8.497 +0.002	cubic spinel single phase	4.1	18
5	1.0	8.522 ±0.001	cubic spinel single phase	4.05	19
6	1.5	8.5265±0.0008	cubic spinel single phase	4.45	10

coefficient and R a thermal contact resistance between the sample and the silver blocks.

In the measurement of thermal conductivity, about 10 g silver block was used on the sample as thermal sink and the thermal conductivity was calculated using equation (1) with the correction term $C_s\rho_s Y$, and the precision was within ±5% in each case. In the measurement of thermal diffusivity, the about 3 g silver block was used and the thermal diffusivity was calculated using equation (2) with the correction term $Z/C_s\rho_s$, the precision was within ±10%. In these calculations, as specific heat capacity of the sample, the data measured recently in our laboratory[17] were used. The temperature difference ΔT was measured by the chromel-alumel sheathed thermocouples, and the sample was in contact with the silver blocks through a layer of silver paste and the two pieces were bound firmly together with thin molybdenum wire (0.2 mm dia.). The apparatus was cooled to about 150 K with liquid nitrogen and then measurement was carried out in the temperature range from 200 to 700 K under a vacuum of 1 Pa.

The thermal conductivity λ_p and diffusivity κ_p with porosity P were corrected to zero porosity λ and κ using Eucken's equation[18] as follows,

$$\lambda = \lambda_p(1 + 0.5P)/(1 - P), \quad (3)$$

and $$\kappa = \kappa_p(1 + 0.5P). \quad (4)$$

3. Results and Discussion

3.1 Thermal diffusivity

The thermal diffusivities of $Mn_xFe_{3-x}O_4$ samples with x values of 0.8, 1.0 and 1.5 are shown in Fig. 1-a, where a λ-type anomaly is observed in each sample. The peak temperatures of the samples with $x = 0.8$, 1.0, 1.5 were 619 ± 4, 570 ± 3 and 474 ± 3 K, respectively. These temperatures are plotted against x and compared with Curie points obtained from magnetic permeability measurement by Gerber *et al.*[1] and Abgrall *et al.*[2] as shown in Fig. 1-b. In the range of $x \geq 1$, the peak temperatures obtained from our thermal diffusivity measurement were in good agreement with Curie points reported by Gerber *et al.*, and in the range of $x < 1$, with those obtained by Abgrall *et al.* The Curie points reported by Gerber *et al.* are not in agreement with those by Abgrall *et al.* and ours. This disagreement would originate from that the cation distributions in tetrahedral and octahedral sites are different between both of the samples.

3.2 Thermal conductivity

The thermal conductivities of polycrystalline magnetite (Fe_3O_4) and hematite (Fe_2O_3) are shown in Fig. 2, together with the results on

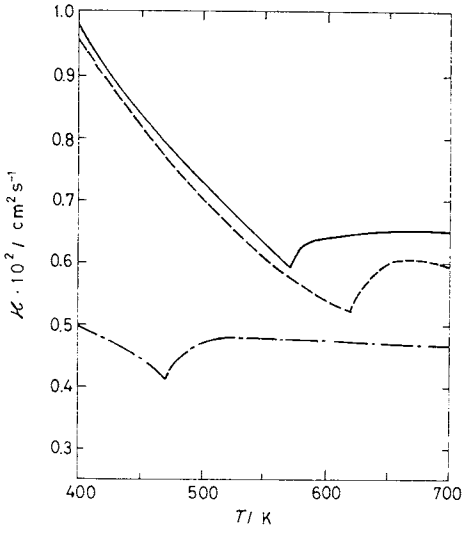

Fig. 1-a Thermal diffusivity of $Mn_xFe_{3-x}O_4$
——— $MnFe_2O_4$;
– – – – $Mn_{0.8}Fe_{2.2}O_4$;
—·—·— $Mn_{1.5}Fe_{1.5}O_4$.

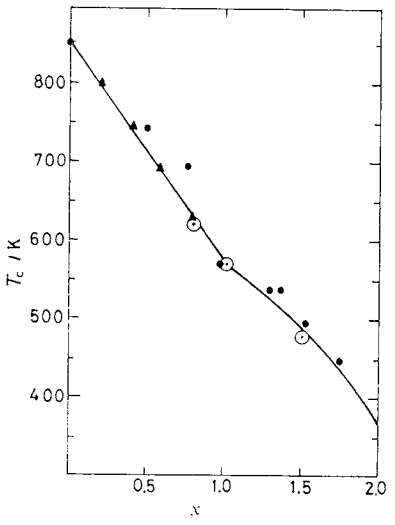

Fig. 1-b Composition dependence of Curie point T_c on $Mn_xFe_{3-x}O_4$
⊙ this work; ● Gerber *et al.*[1];
▲ Abgrall *et al.*[2].

polycrystalline and single crystal of magnetite by Kamilov *et al.*[19] and those on single crystal of magnetite by Slack[20]. Our results on polycrystalline magnetite are in good agreement with the results by Kamilov *et al.* up to 300 K, but the thermal conductivities of single crystal of magnetite by Kamilov *et al.* and Slack are higher than our results on polycrystals. The thermal conductivity of natural crystal of hematite reported by Koenigsberger *et al.* ($0.147\ \mathrm{W\,cm^{-1}\,K^{-1}}$ at 303 K)[21] is also higher than our polycrystalline data. In our measurements, the thermal conductivity of magnetite is about half of that of hematite. This is analogous to the result obtained by Slack[20] that the thermal conductivity of $MgAl_2O_4$ is lower than of α-Al_2O_3, where Fe_3O_4 has the same spinel structure as $MgAl_2O_3$ and Fe_2O_3 the same rhombohedral structure as α-Al_2O_3.

The each thermal conductivity of polycrystalline $Mn_xFe_{3-x}O_4$ (x = 0.25, 0.5, 0.8, 1.0, 1.5) is shown in Fig. 3. The results of $MnFe_2O_4$ single crystal by Shchelkotunov *et al.*[8] indicated by a dashed curve in Fig. 3 are higher than our results of $MnFe_2O_4$ polycrystal. The thermal conductivities of $Mn_xFe_{3-x}O_4$ with x of 0.25, 0.5 and 1.5 are observed nearly independent to the temperature, and lower than $MnFe_2O_4$, as shown in Fig. 3. T_c indicated by an arrow shows the peak temperature observed by the thermal diffusivity measurement. The anomaly in thermal conductivity at the magnetic transition was hardly observed for x=0.8, but not for x =1.0 and 1.5.

3.3 Apparent phonon mean free path

The thermal transport of ferrites can be considered consisting of the contributions of phonon and magnon[22-24], and thus the thermal conductivity is expressed by using the mean free path concept as follows:

$$\lambda = \lambda_L + \lambda_m = (C_L u_L l_L + C_m u_m l_m)/3 \qquad (5)$$

where λ, C, u and l are thermal conductivity, heat capacity per unit volume, mean velocity and mean free path, respectively, and the suffix L and m denote the contribution of phonon and magnon, respectively.

In the range of magnetic transition temperature, the two cases would be considered: the one is such that λ_m increases due to λ-type magnon heat capacity C_m[23,24] and the other is that λ_L decreases due to the scattering of phonon with magnon[25]. Kamilov *et al.* have reported that the thermal conductivity of $Cu_{0.4}Cd_{0.6}Fe_2O_4$ decreases anomalously near the Curie point, where λ_L of lattice contribution changes abruptly by the

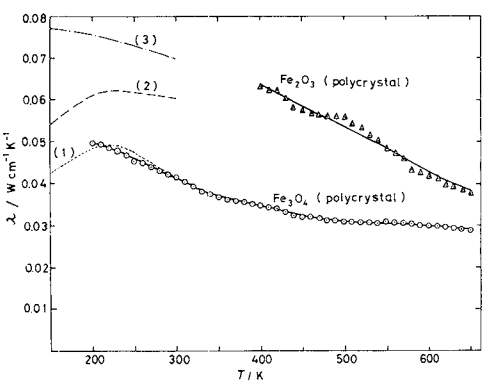

Fig. 2 Thermal conductivities of magnetite and hematite
- ⊙ polycrystalline magnetite (this work);
- △ polycrystalline hematite (this work);
- 1: polycrystalline magnetite by Kamilov *et al.*[19];
- 2: single crystal magnetite by Kamilov *et al.*[19];
- 3: single crystal magnetite by Slack[20].

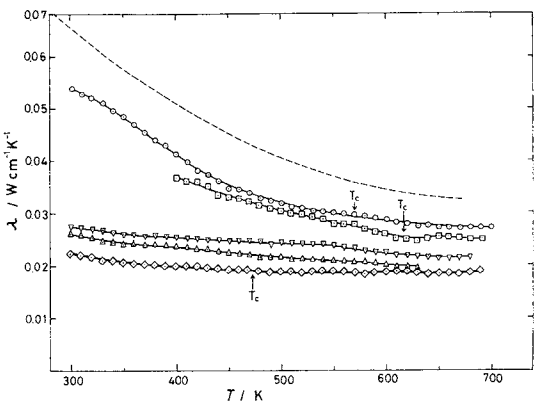

Fig. 3 Thermal conductivity of $Mn_xFe_{3-x}O_4$
- △ $Mn_{0.25}Fe_{2.75}O_4$; ▽ $Mn_{0.5}Fe_{2.5}O_4$;
- ⊡ $Mn_{0.8}Fe_{2.2}O_4$; ⊙ $MnFe_2O_4$;
- ◇ $Mn_{1.5}Fe_{1.5}O_4$;
- --- $MnFe_2O_4$ by Shchelkotunov *et al.*[8].
- T_c: Curie point observed by the thermal diffusivity measurement.

scattering of phonon with magnon while λ_m of spin contribution is negligibly small[19,26]. In the case such as $Cu_{0.4}Cd_{0.6}Fe_2O_4$, it is considered that magnon strongly couples with phonon and then spin-lattice relaxation time near the Curie point is relatively short; from 4.5×10^{-8} to 1.77×10^{-8} s[27]. On the other hand, in the case of ferromagnetic solid EuO, its thermal diffusivity decreases anomalously near the Curie point[28] while the thermal conductivity does not change clearly in this region[28,29] in the same manner as the case of Mn-ferrites. These temperature dependences in EuO have been explained to be due to the long spin-lattice relaxation time by Huber[30]. In this case, phonon is scarcely scattered by magnon and moreover thermal transport by spin modes is extremely small, and then the thermal conductivity does not change clearly near the Curie point[28]. Consequently it would be considered in the case of Mn-ferrite that spin-lattice relaxation time is relatively long and that phonon contribution of thermal conductivity is dominant. The anomalous decrease of the thermal diffusivity of Mn-ferrite can be explained through the relation $\kappa = \lambda / C_p \rho$ (C_p: heat capacity per unit mass).

Assuming that thermal conductivity of Mn-ferrite is expressed by only phonon contribution λ_L of the first term in equation (5) and its sound velocity u_L is constant (3.5×10^5 cm/s) in the temperature range under the measurement, the phonon mean free path was calculated from equation (5), where the lattice heat capacity of $Mn_xFe_{3-x}O_4$ was calculated from Debye temperature estimated from four prominent infra-red absorption bands[6,7,31]. Apparent phonon mean free path thus obtained was plotted against $1/T$ for $Mn_xFe_{3-x}O_4$ as shown in Fig. 4. Each apparent phonon mean free path is very low and decreases with increase in temperature and becomes comparable with the lattice spacing. Similar results may also be seen in some other spinel-ferrites[8,19,23,24,26] above room temperature except near the Curie point, considering their low thermal conductivity data. And the difference in the apparent phonon mean free paths for various metal composition may originate from the cation distribution as will be discussed in the following section.

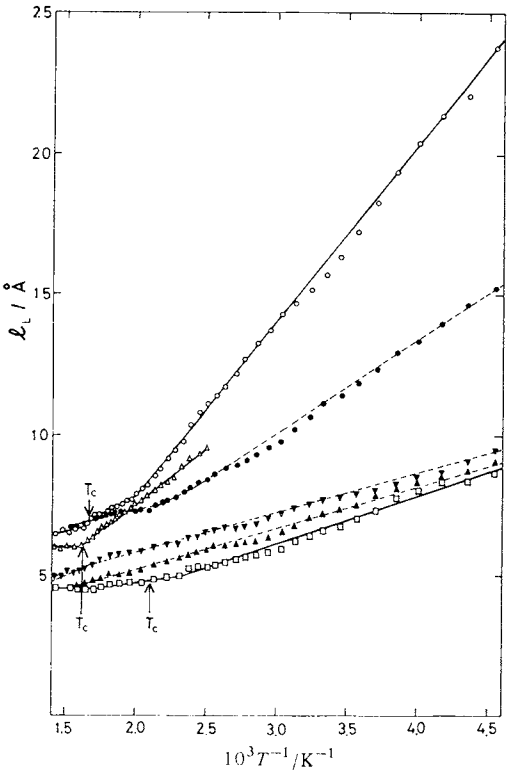

Fig. 4 Apparent phonon mean free path of $Mn_xFe_{3-x}O_4$ and magnetite
--●-- Fe_3O_4 (magnetite);
--▲-- $Mn_{0.25}Fe_{2.75}O_4$;
--▼-- $Mn_{0.5}Fe_{2.5}O_4$;
—△— $Mn_{0.8}Fe_{2.2}O_4$;
—○— $MnFe_2O_4$;
—□— $Mn_{1.5}Fe_{1.5}O_4$;
T_c: Curie point observed by thermal diffusivity measurement.

3.4 Composition dependence of thermal conductivity

Composition dependence of thermal conductivity of $Mn_xFe_{3-x}O_4$ at each temperature is shown in Fig. 5. Here, two maxima are observed at the composition $x = 0$ and 1.0. It has been known that the lattice constant[5,6,16] and electrical[1,32,33] and magnetic properties[1] change their dependences on the metal composition of $Mn_xFe_{3-x}O_4$ at $x = 1$, which originate from the cation distribution in the lattice of spinel. Lotgering *et al.* have suggested on the cation distribution of Mn-ferrites from the measurements of the electrical conductivity, the Seebeck voltage[33] and the Mössbauer spectra[34] as follows,

$$Mn^{2+}_{1-\gamma}Fe^{3+}_{\gamma}\ [Mn^{2+}_{x+\gamma-1}Fe^{2+}_{1-x}Fe^{3+}_{2-\gamma}]O_4 \quad (0 \leq x \leq 1.0), \qquad (6)$$

$$Mn^{2+}_{1-\gamma}Fe^{3+}_{\gamma}\ [Mn^{2+}_{\gamma}Mn^{3+}_{x-1}Fe^{3+}_{3-\gamma-x}]O_4 \quad (1.0 \leq x \leq 1.9), \qquad (7)$$

where cations in square blackets occupy octahedral sites, the others tetrahedral sites, and γ denotes the amounts of Fe^{3+} ions on tetrahedral sites. The composition dependence of γ changes at $x = 1$, and moreover at $x > 1$ Fe^{3+} ions and Mn^{2+} ions on octahedral sites are replaced by Mn^{3+} ions. For the cubic ferrites with $x > 1$, it was also concluded by Brabers from the splitting of the infra-red absorption bands that there are local tetragonal distortions originating from the Jahn-Teller effect of the octahedral Mn^{3+} ions[6].

Now, the solid solution model of thermal conductivity proposed by Abeles[35] would be applied to the system of Fe_3O_4-$MnFe_2O_4$. According to this theory the scattering of phonons in the mixed substances depends on a scattering cross section, which is expressed by

$$\Gamma \sum_i x_i \{(M_i - M)/M\}^2 + \varepsilon\{(\delta - \delta_i)/\delta\}^2\}, \qquad (8)$$

where x_i is the fractional concentration of the component i of solid solution, and M and δ are the average mass and radius per unit atom of solid solution, and M_i and δ_i are the atomic mass and radius when the host lattice is wholly occupied by i-th atom, and ε should be regarded as a phenomenological adjustable parameter originated from the bond of the lattice. The cation radii of Mn^{2+}, Mn^{3+}, Fe^{2+} and Fe^{3+} ions in $Mn_xFe_{3-x}O_4$ have been given 0.91, 0.7, 0.83 and 0.67 Å by Gorter[36], respectively. In the range from $x = 0$ to 1.0, the scattering cross section Γ could be calculated using equation (8) from the cation distribution obtained in formula (6) using γ value reported by Rieck *et al.*[5] on the octahedral and tetrahedral sites, and then the results are shown in Fig. 6, where ε on each site is assumed to be 40[35]. In Fig. 6 there is a maximum between 0.4 and 0.5 of x value, which comes from the large difference of the radius between Mn^{2+} and Fe^{3+} ion on the tetrahedral site.

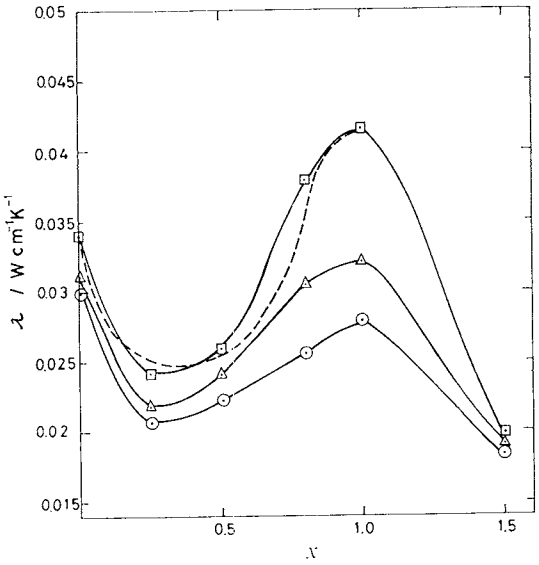

Fig. 5 Composition dependence of thermal conductivity on $Mn_xFe_{3-x}O_4$
● 400 K; △ 500 K; ⊙ 600 K;
The dashed curve was computed from equation (9) using $\Delta\Gamma$ as shown in Fig. 6 with $\alpha = 2.5$, $\varepsilon = 40$ at 400 K.

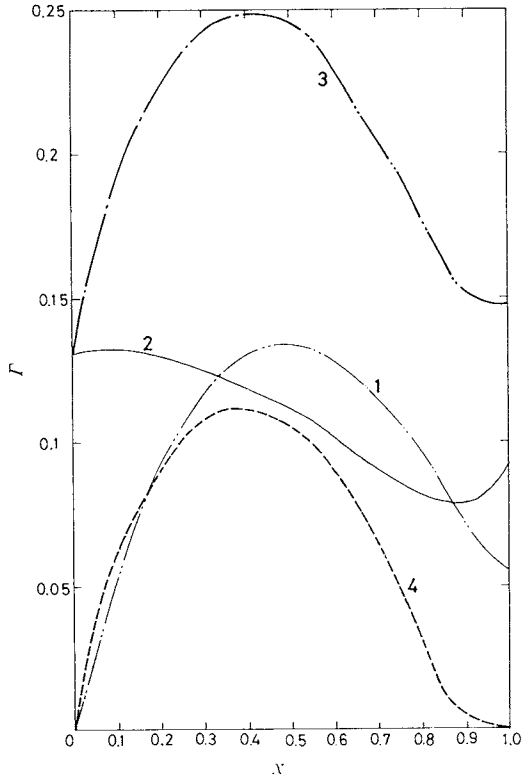

Fig. 6 Calculated phonon scattering cross section of the cation components on $Mn_xFe_{3-x}O_4$
1: tetrahedral site; 2: octahedral site; 3: 1 + 2; 4: $\Delta\Gamma$ (substraction of the base line from curve 3.).

The composition dependence of thermal conductivity shown in Fig. 5 is mainly explained by the cation distribution on the tetrahedral site, since thermal resistance independent of temperature is proportional to Γ. In the next place we should estimate the thermal resistance R in this solid solution from Γ using the method by Abeles[35]. Abeles has derived the following equation:

$$\frac{R}{R_0} = (1+5\alpha/9)\left(\frac{\tan^{-1}U}{U}\right. + \frac{\left(1-\frac{\tan^{-1}U}{U}\right)^2}{\left(\frac{1+\alpha}{5\alpha}\right)U^4 - U^2/3 + 1 - \frac{\tan^{-1}U}{U}}\left.\right)^{-1} \quad (9)$$

where $U^2 = (1+5\alpha/9)^{-1}(9\pi/2)^{1/3}(\pi h/2)k^{-2}\theta^2\Delta\Gamma\theta^{-1}R_0^{-1}$, h Planck's constant, k Boltzmann constant, θ Debye temperature, R_0 the thermal resistance in the absence of point defect scattering created by solid solution and α the ratio of normal to Umklapp process. Here, we define $\Delta\Gamma$ as $\Gamma - \Gamma_0$ (Γ_0 is the scattering cross section in the absence of point defect created by solid solution.), and it is shown by a dashed curve in Fig. 6. Assuming $\alpha = 2.5$[35], the composition dependence of thermal conductivity can be calculated from $\Delta\Gamma$ using equation (9) and the results at 400 K are shown by a dashed curve in Fig. 5 as an example. The calculated values are fairly in good agreement with the experimental results in the range from $x = 0$ to 1.0

For the region from $x = 1.0$ to 1.9, Γ can be calculated in the same way, but the calculated Γ decreases as the composition x increases, contrary to the experimental results. The reason for this discrepancy is not clear at present but the presence of local tetragonal distortions due to Jahn-Teller effect of the octahedral Mn^{3+} ions may result in the increase of $\Gamma_{Mn^{3+}}$. Accordingly, Γ should increase with the increase of Mn^{3+} ions, when the increase by Jahn-Teller distortion compensates for the decrease of Γ due to the solid solution.

Acknowledgment

The authors wish to thank Dr. H. Inaba and Mr. H. Yagi for their valuable comments on this work and also thank Mr. N. Sasaki for his help in sample preparation.

References

1) R. Gerber, Z. Šimša and M. Vichr, *Czech. J. Phys.* B 16, 913 (1966)
2) C. Abgrall, M. Porte and A. Marais, *J. Phys. Chem. Solids* 38, 441 (1977)
3) V. L. Moruzzi, *J. Appl. Phys.* 32, 59S (1961)
4) S. E. Harrison, C. J. Kriessman and S. R. Pollack, *Phys. Rev.* 110, 844 (1958)
5) G.D. Rieck and F.C.M. Driessens, *Acta Cryst.* 20, 521 (1966).
6) V. A. M. Brabers, *Phys. Stat. Sol.* 33, 563 (1969)
7) M. Ishii, M. Nakahira and T. Yamanaka, *Solid State Comm.* 11, 209 (1972)
8) V. A. Shchelkotunov, V. N. Danilov and V. V. Lyukshin, *Izv. Akad. Nauk. SSSR. Neorg. Mater.* 11, 1638 (1975)
9) D. Douthett and S. A. Friedberg, *Phys. Rev.* 121, 1662 (1961)
10) K. Naito, H. Inaba and Y. Noda, *J. Nucl. Sci. Technol.* 13, 508 (1976)
11) Y. Noda and K. Naito, *J. Nucl. Mater.* 66, 17 (1977)
12) L. S. Darken and R. W. Gurry, *J. Am. Chem. Soc.* 68, 798 (1946)
13) K. Ono, T. Ueda, F. Ozaki, Y. Ueda, T. Yamaguchi and G. Moriyama, *Nihon Kinzoku Gakkaishi* 35, 757 (1971)
14) A. Muan, *Am. Mineralogist* 46, 364 (1961)
15) K. Naito, T. Tsuji, Y. Asakura and T. Yamashita, unpublished
16) T. Yamanaka and K. Fujino, *Nihon Kesshou Gakkaishi* 17, 181 (1975)
17) K. Naito, H. Inaba and H. Yagi, unpublished
18) A. Eucken, *Forsh. Gebiete Ingenieurw.* B 3, Forshungsheft No. 353, 16 (1932)
19) I. K. Kamilov, G. M. Shakhshaev, Kh. K. Aliev, G. G. Musaev and M. M. Khamidov, *Zh. Eksp. Teor. Fiz.* 68, 586 (1975)
20) G. A. Slack, *Phys. Rev.* 126, 427 (1962)
21) J. Koenigsberger and J. Weiss, *Ann. Physik* 35, 1 (1911)
22) S. Geller, *J. Appl. Phys.* 40, 1555 (1969)
23) L. A. Fomenko, V. A. Shchelokotunov and V. L. Sochivko, *Sov. Phys. Solid State* 5, 643 (1963) *Fiz. Tverd. Tela* 5, 874 (1963)
24) C. Ferro, C. Piconi and F. Sellari, Adv. Therm. Conduct. Pap. Int. Conf. Therm. Conductivity 12th 398 (1974)
25) H. Stern, *J. Phys. Chem. Solids* 26, 153 (1965)
26) K. Kamilov, G. M. Shakhshaev and M. Khamidov, *Sov. Phys. Solid State* 17 191 (1975) *Fiz. Tverd. Tela* 17, 316 (1975)
27) K. Kamilov, Kh. K. Aliev and G. M. Shakhshaev, *Sov. Phys. Solid State* 15 632 (1973)

Fiz. Tverd. Tela **15**, 914 (1973)
28) M. B. Salamon, P. R. Garnier, B. Golding and E. Buehler, *J. Phys. Chem. Solids* **35**, 851 (1974)
29) J. J. Martin and G. S. Dixon, *Phys. Stat. Sol.* (b) **54**, 707 (1972)
30) D. L. Huber, *Phys. Rev.* B **3**, 836 (1971)
31) N. W. Grimes, *Phil. Mag.* **25**, 67 (1972)
32) Z. Šimša, *Czech. J. Phys.* B **16**, 919 (1966)
33) F. K. Lotgering, *J. Phys. Chem. Solids* **25**, 95 (1964)
34) F. K. Lotgering and A. M. Van Diepen, *J. Phys. Chem. Solids* **34**, 1369 (1973)
35) B. Abeles, *Phys. Rev.* **131**, 1906 (1963)
36) E. W. Gorter, *Philips Res. Rep.* **9**, 295 (1954)